A single vesicle fluorescence microscopy platform to quantify phospholipid scrambling

Sarina Veit[1], Grace I. Dearden[2], Kartikeya M. Menon[3], Faria Noor[2], Anant K. Menon[2,*], Thomas Günther Pomorski[1,4,*]

[1]Department of Molecular Biochemistry, Faculty of Chemistry and Biochemistry, Ruhr University Bochum, Bochum 44801, Germany

[2]Department of Biochemistry, Weill Cornell Medical College, New York, New York 10021, USA

[3]Icahn School of Medicine at Mount Sinai, New York, NY 10029

[4]Department of Plant and Environmental Sciences, University of Copenhagen, DK-1871 Frederiksberg C, Denmark

* To whom correspondence should be addressed: Anant K. Menon (Tel: +1-646-962-2476; Email: akm2003@med.cornell.edu) and Thomas Günther-Pomorski (Tel: +49 2343224430; Email: Thomas.Guenther-Pomorski@ruhr-uni-bochum.de)

Running head: Single vesicle analysis of VDAC scrambling

Keywords: NBD-phospholipid, Proteoliposome, Scramblase, Single vesicle, TIRF microscopy

Abstract

Scramblases play important roles in physiology by translocating phospholipids bidirectionally across cell membranes. For example, scrambling facilitated by VDAC1 dimers is the primary mechanism by which endoplasmic reticulum-derived phospholipids cross the outer membrane to enter mitochondria. Precise quantification of lipid scrambling, while critical for mechanistic understanding, cannot be obtained from ensemble averaged measurements of the activity of reconstituted scramblases. Here, we describe a microscopy platform for high-throughput imaging of single vesicles reconstituted with fluorescently-labeled phospholipids and heterogeneously crosslinked VDAC1 dimers. For each vesicle, we quantify size, protein occupancy and scrambling rate. Notably, we find that individual VDAC1 dimers have different activities, ranging from <100 to >10,000 lipids per second. This kinetic heterogeneity, masked in ensemble measurements, reveals that only some dimer interfaces are capable of promoting rapid scrambling, as suggested by molecular dynamics simulations. Our platform provides a versatile framework for quantifying scramblases and exploring their regulation.

Introduction

Scramblases facilitate the bidirectional translocation of polar lipids across cell membranes, a fundamental process that supports many aspects of cellular life. In metazoan cells, lipid scrambling is required for the exposure of the signaling molecule phosphatidylserine at the cell surface during apoptosis or upon cell activation, expansion of the endoplasmic reticulum (ER) and autophagosomal membranes, lipoprotein assembly, and all forms of protein glycosylation in the ER [1–7]. Members of the G protein-coupled receptor (GPCR) [8] and TMEM16 [9,10] families were the first scramblases to be identified at the molecular level based on the demonstration of their scrambling activity after purification and reconstitution into unilamellar liposomes.

We recently reported that the mitochondrial β-barrel protein VDAC1 is a scramblase that provides the primary mechanism by which phospholipids, arriving at the mitochondrial surface from the ER via bridge-like transfer proteins [11], cross the outer membrane to enter mitochondria [12]. Phospholipid import is needed to grow the double membrane system of mitochondria and provide precursors for the biosynthesis of cardiolipin, a tetra-acylated lipid that is necessary for mitochondrial function, as well as phosphatidylethanolamine which is needed in mitochondria but also distributed to other cellular membranes [13,14]. Molecular dynamics simulations indicated that lipid scrambling is facilitated by VDAC1 dimers and occurs efficiently only at a specific dimer interface among several possible dimer configurations [12]. To test this experimentally, we used an amine-reactive crosslinker to generate a mixture of unique VDAC1 dimers, including a subset with a suitable interface for lipid scrambling. When reconstituted into liposomes, ensemble average measurements revealed that the crosslinked VDAC1 preparation scrambled lipids, whereas the non-crosslinked protein was inactive unless reconstituted at a sufficiently high protein-to-phospholipid ratio to allow spontaneous dimer formation [12]. Given that VDAC1 is the most abundant protein in the mitochondrial outer membrane, with a density of >1,000 molecules per μm^2 of surface [15], it is likely that scrambling-active native dimer interfaces are likely to be formed by molecular crowding.

Despite advances in the purification, reconstitution and assay of lipid scramblases their functional and mechanistic characterization remains a challenge. Current

approaches typically involve reconstituting these proteins into large unilamellar liposomes (approximately 200 nm in diameter) with defined bulk lipid compositions, followed by ensemble-averaged biophysical or biochemical studies. However, a fundamental limitation of ensemble measurements is the inherent heterogeneity of liposome preparations. Variability in size, lamellarity, membrane integrity, lipid composition, protein copy number, and protein orientation [16–18] complicates ensemble data interpretation by masking the dynamics of individual proteins. Such measurements also yield only average transport kinetics limiting the resolution and specificity of the analysis.

A single report in the literature describes an elegant attempt to overcome these challenges by analyzing the scramblase activity of Ca^{2+}-activated TMEM16F in a microarray format, wherein purified protein is reconstituted into bespoke fabricated microchambers with an asymmetric bilayer consisting of a unique inner leaflet and an outer leaflet common to the entire microarray [19]. Activation of the scramblase results in lipid transfer from the outer leaflet to the inner leaflet of the microchamber, which is tracked using fluorescent lipid reporters. Notably, these experiments yielded a unitary rate for TMEM16F-mediated scrambling, but the technical complexity of the set-up and demanding experimental workflow limit its practicality to specialized applications.

We now report a readily implementable, high-throughput single-vesicle assay to study scramblase activity, using dimeric human VDAC1 as an exemplar of scramblase proteins. We reconstituted vesicles with a fluorescent phospholipid reporter and fluorescently labeled, chemically crosslinked VDAC1 dimers, deposited the vesicles on a passivated glass slide and used total internal reflection fluorescence (TIRF) microscopy to resolve individual vesicles. This approach enables a detailed characterization of the reconstituted proteoliposome ensemble, wherein we quantify vesicle size, protein occupancy, and lipid scrambling at the single-vesicle level using a novel adaptation of the common bovine serum albumin (BSA) back-extraction assay [20,21]. By identifying vesicles containing a single VDAC1 dimer, we could obtain a unitary scrambling rate. Notably, because our dimer preparation is heterogeneous, we found that some dimers were inactive while others scrambled lipids at rates ranging from <100 to >10,000 lipids per second. This kinetic heterogeneity, which is masked in ensemble measurements, reveals that only a subset of dimer interfaces is capable

of rapidly scrambling lipids, consistent with predictions from molecular dynamics simulations [12]. Our platform can be readily modified and extended to quantify other scramblases and learn, for example, how their activity is regulated by membrane lipid composition [17]. It can also be used to study ATP-driven lipid transporters, i.e. flippases and floppases [22,23], providing a powerful and customizable method for their functional characterization.

RESULTS

Single vesicle phospholipid scramblase assay

The fluorescent phospholipid analog 14:0-6:0 NBD phosphatidylcholine (NBD-PC) (Extended Data Fig. 1a) is commonly used as a reporter in 'back-extraction' phospholipid scramblase assays (Extended Data Fig. 1b)[20,21,24] due to its ability to desorb from membranes (rate constant ~0.07 s^{-1}, Extended Data Fig. 1c,d) into aqueous media where it has slight solubility (~0.75 μM, Extended Data Fig. 1e). In such assays, unilamellar vesicles containing trace amounts of NBD-PC are incubated with excess albumin. When NBD-PC desorbs from the outer leaflet of the vesicle, albumin captures it within its hydrophobic binding pockets, leading to a decrease in fluorescence because the NBD fluorophore has a lower quantum efficiency when associated with albumin than in the membrane (Extended Data Fig. 1b). For protein-free vesicles, where lipids do not scramble within the time-frame of the experiment, fluorescence quenching is partial as inaccessible NBD-PC molecules in the inner leaflet of the vesicles are retained while those in the outer leaflet are captured by albumin (Extended Data Fig. 1c). However, if a vesicle possesses an active scramblase, NBD-PC molecules in the inner leaflet are translocated to the outer leaflet, ultimately allowing all NBD lipid to be captured resulting in maximal fluorescence quenching (Extended Data Fig. 2f, 'CL' trace). Building on this well-characterized system, we developed a new method to visualize VDAC1-mediated phospholipid scrambling in single vesicles.

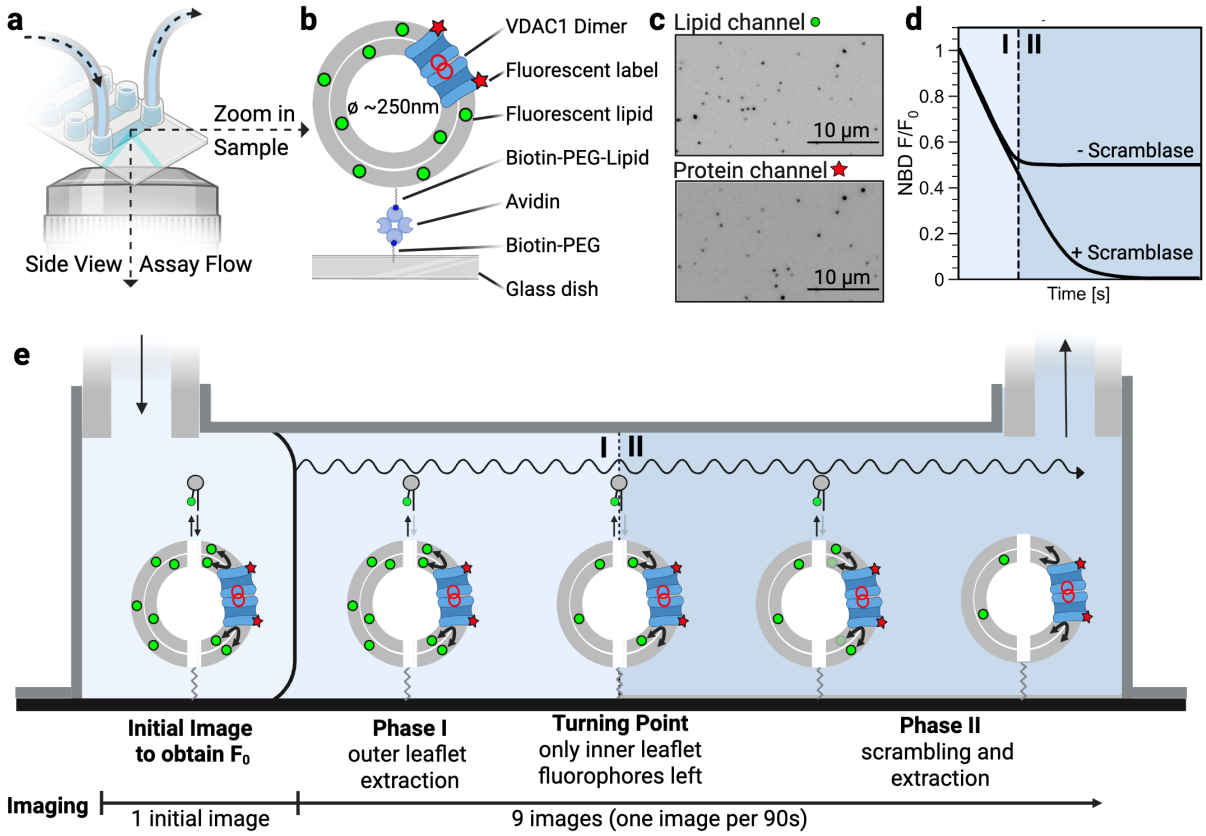

Figure 1: Single vesicle scramblase assay. a, Illustration of the sample chamber, with tubing for flushing, depicted in the context of a TIRF microscope objective lens. **b**, Illustration of a single vesicle, containing an Alexa647-labeled VDAC1 dimer and a trace quantity of fluorescent lipid (14:0-6:0 NBD-PC), immobilized on a polymer-passivated (PLL-g-PEG/PLL-g-PEG-biotin) glass coverslip via biotin-neutravidin tethering. **c**, Representative TIRF images of immobilized vesicles visualized in the lipid channel (NBD) and protein channel (Alexa647). The lipid signal serves as a read-out of scramblase activity, while the protein signal estimates the number of proteins per vesicle. **d**, Theoretical fluorescence traces for individual immobilized liposomes with and without scramblase activity according to the protocol described in panel e. **e**, Schematic presentation of the assay steps. After vesicle immobilization, continuous buffer flow (wavy line) in the imaging chamber removes 14:0-6:0 NBD-lipids that readily partition from the vesicle outer leaflet into the buffer (phase I). At this juncture (turning point) vesicles contain 14:0-6:0 NBD-lipids only in the inner leaflet. Next, in phase II of the sequence, these remaining 14:0-6:0 NBD-lipids are flipped to the outer leaflet in scramblase-containing vesicles where they become accessible to buffer extraction. Note that these phases partially overlap. Vesicles are depicted to illustrate the outcome for liposomes with a scramblase (right half) or without a scramblase (left half).

The protocol requires vesicles containing the NBD-PC reporter, a biotinylated anchor lipid, and fluorescent VDAC1dimers (control vesicles would lack protein). Using a flow chamber (Fig. 1a), the vesicles would be immobilized on a passivated glass slide via biotin-neutravidin interaction (Fig. 1b) and imaged by total internal reflection fluorescence (TIRF) in both lipid and protein fluorescence channels (Fig. 1c). Under

these conditions, a small pool of NBD-PC should be in equilibrium between the aqueous phase and the vesicle membrane (Fig. 1e). On flowing buffer through the sample chamber, this aqueous pool of NBD-PC should be washed away, driving the progressive depletion of outer-leaflet NBD-PC as it continues to desorb into solution (Fig. 1d/e, 'Phase I'). Thus, initially, all vesicles will lose their complement of outer leaflet NBD-PC, resulting in a ~50% loss of fluorescence. In vesicles with scramblase activity, inner leaflet NBD-PC translocates outwards, desorbs, and is washed away, resulting in complete loss of fluorescence (Fig. 1d/e, 'Phase II'). If scrambling is slower than outer-leaflet depletion, the two processes can be deconvoluted, yielding a scrambling rate constant. By identifying vesicles equipped with a single VDAC1 dimer, and knowing the size of the vesicle and therefore the number of phospholipids it contains, we would be able to determine the unitary rate of VDAC1-mediated scrambling.

Validation of the experimental platform

We validated our proposed experimental platform in two ways. First, we confirmed that NBD-lipids would be lost from the outer leaflet via desorption and buffer flow, resulting in a predictable loss of fluorescence from individual vesicles. To test this, we prepared liposomes labeled symmetrically with NBD-PC, or with head-labeled *N*-NBD-PE which cannot desorb as it has two long acyl chains which confine it to the membrane. We also prepared liposomes labeled asymmetrically with NBD-PC located only in the outer leaflet. After depositing the liposomes in the sample chamber, we initiated imaging and buffer flow. *N*-NBD-PE labeled liposomes maintained a relatively stable fluorescence signal throughout the assay (Fig. 2a), consistent with the lipid remaining associated with the vesicles throughout the time course. In contrast, liposomes asymmetrically labeled with NBD-PC showed a complete loss of fluorescence within the first 200 s (Fig. 2b). Finally, liposomes symmetrically labeled with NBD-PC, showed an initial rapid decrease in fluorescence (within the first 200 s), reaching a plateau at 41.0 ± 8.8 % of the initial signal, corresponding to the non-extractable lipid pool in the inner leaflet (Fig. 2c and Extended Data Fig. 1f). Mono-exponential fitting of the fluorescence decay traces yielded a rate constant γ~0.012 ± 0.005 s^{-1} (Extended Data Fig. 1g), characterizing the composite process of NBD-PC desorption and buffer flow removal. This value is ~3-fold smaller than the desorption rate constant determined in bulk

assays (Extended Data Fig. 1d) but nevertheless within the same order of magnitude. We note that the rate of fluorescence loss in the single vesicle system depends on flow conditions; we optimized the flow rate to balance efficient desorption with minimal disturbance to the microscope stage and image focus.

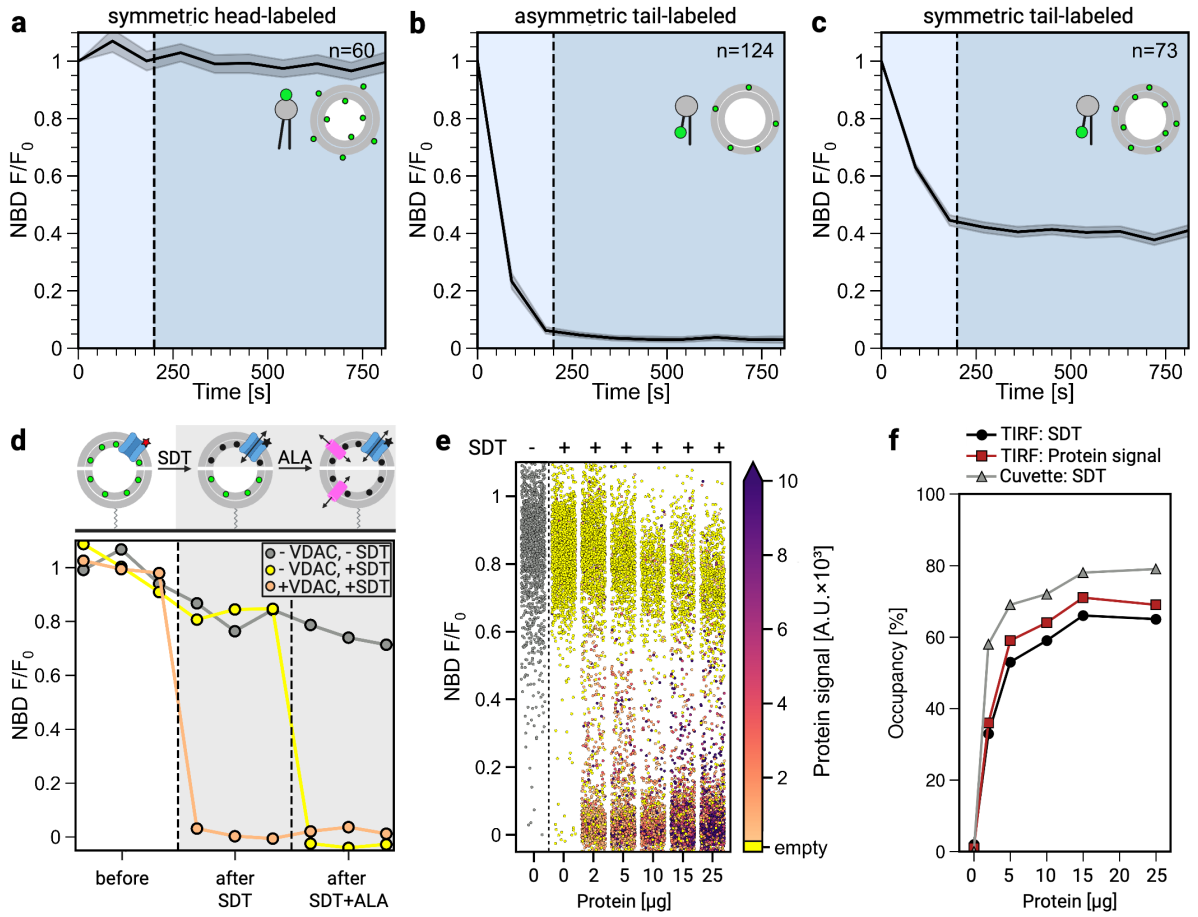

Fig. 2. Verification of the single vesicle scramblase assay platform. a-c, Liposomes labeled symmetrically or asymmetrically with the indicated NBD-lipids were immobilized as in Figure 1b,e. TIRF microscopy imaging was started simultaneously with buffer flow (t=0 min). For each vesicle, lipid fluorescence intensity was normalized to the corresponding initial intensity, and individual traces were combined into a plot showing the mean ± SD (the number of averaged individual liposome traces is indicated at the top right of the graphs). **a**, Symmetrically labeled liposomes with head-labeled *N*-NBD-PE in both leaflets. **b**, Asymmetrically labeled liposomes with 14:0-6:0 NBD-PC in the outer leaflet. **c**, Symmetrically labeled liposomes with 14:0-6:0 NBD-PC in both leaflets. **d**, 14:0-6:0 NBD-PC-containing proteoliposomes reconstituted with non-crosslinked Alexa647-labeled VDAC1 were imaged by TIRF microscopy alongside protein-free liposomes to determine reconstitution efficiency. After vesicle immobilization, buffer flow was used to remove outer-leaflet NBD lipids. This was followed by sodium dithionite (SDT) addition to selectively bleach inner-leaflet NBD lipids in VDAC1-containing vesicles. Alamethicin (ALA) was then added to permeabilize all vesicles, confirming complete bleaching. Exemplary fluorescence traces are shown for a vesicle containing supposedly one protein (orange) and a protein-free liposome (yellow). The control without SDT accounts for photobleaching effects (grey). **e**, NBD fluorescence intensity of individual vesicles reconstituted with the indicated amounts non-crosslinked VDAC1 after

dithionite addition, with the initial protein signal indicated by a colormap (scale on the right; the protein colormap corresponds to the initial Alexa647 fluorescence of the vesicles as this fluorophore is also bleached on SDT treatment). The control sample indicated in the first column was not subjected to SDT treatment. **f**, Comparison of vesicle protein occupancy determined by dithionite single vesicle assay (black), single vesicle protein signal (red) and bulk dithionite assay in cuvette (grey). The x-axis represents the amount of protein used per reconstitution.

We next confirmed that the experimental platform recapitulated previously reported ensemble data on VDAC1 reconstitution. Specifically, we quantified the lipid and protein content of each vesicle and determined the fraction of vesicles functionalized with a VDAC1 channel. We then related this information to the amount of protein used for reconstitution. Thus, we purified a single-cysteine variant of VDAC1 (Extended Data Fig. 2a,b) in which the cysteine residue (A170C) faces the aqueous pore of the β-barrel where it does not interfere with scramblase activity. We then labeled the A170C site with Alexa647-maleimide at high (>97%, Extended Data Fig. 2c) efficiency and reconstituted the protein into liposomes containing NBD-PC. Under these conditions, VDAC1 functions principally as a channel as its scramblase activity requires dimerization, which can be achieved by chemical crosslinking (see later). The resulting proteoliposomes were immobilized onto a TIRF microscope channel slide (Fig. 1a,b) and flushed with buffer for 5 min to remove NBD-PC molecules from the outer leaflet. After stopping buffer flow, the sample was imaged to determine the initial lipid and protein fluorescence of each vesicle. We next added sodium dithionite (SDT), a membrane impermeant reductant which reacts with NBD fluorophores to eliminate their fluorescence (Fig. 2d,e) and measured the remaining fluorescence in each vesicle [18]. Finally, we added the SDT-permissive pore-forming peptide alamethicin (Fig. 2d and Extended Data Fig. 3) to expose all pools of NBD-PC to SDT[18].

NBD-PC molecules in the inner leaflet of protein-free vesicles are inaccessible to SDT and consequently these vesicles are expected to retain their fluorescence until the addition of alamethicin which allows SDT to enter the vesicles (Fig. 2d, top panel). On testing the flow protocol with protein-free vesicles in the absence of dithionite, we observed some fluorescence loss (~15%) due to desorption/flushing of residual NBD-PC from the outer leaflet which had not been completely removed during the initial phase of the experiment (Fig. 2d, bottom panel, grey trace marked '-VDAC, -SDT'; also Fig. 2e, first column). A similar loss was seen on SDT treatment of protein-free

vesicles (Fig. 2d, bottom panel, yellow trace; Fig. 2E, second column, labeled 0 µg protein). Adding a correction for this technical effect, we next calculated the proportion of vesicles with less than 45% of their initial lipid fluorescence left after SDT addition. As SDT can enter vesicles through the VDAC1 pore, it should eliminate all NBD-PC fluorescence in VDAC1-containing vesicles. Indeed, we observed essentially complete loss of NBD fluorescence upon dithionite addition in vesicles with a signal approximately >300 in the Alexa647 channel, indicating that this threshold is a reliable estimate of the minimum fluorescence signal of a single Alexa647-VDAC1 protein.

Reconstitution of VDAC1 into vesicles is proposed to follow Poisson statistics, meaning the fraction of vesicles containing one or more VDAC1 molecules should correlate with the amount of protein used. To test this, we prepared vesicles with different protein/phospholipid ratios and used Alexa647 imaging to measure directly the percentage of vesicles containing at least one VDAC1 copy (i.e., vesicles with an Alex647 signal >300 units). We treated the immobilized samples with SDT, as described above, to determine the fraction of vesicles that lost their entire NBD fluorescence, indicating the presence of at least one functional VDAC1 channel. When graphed as a function of the amount of Alexa647-VDAC1 used for reconstitution, both the direct measurement of Alex647 fluorescence intensity of vesicles (Fig. 2f, red circles) and the functional read-out obtained via SDT-mediated bleaching (Fig. 2f, black circles) yielded identical profiles. We compared these single vesicle approaches with results obtained from bulk assays where SDT treatment was used to infer the fraction of vesicles containing VDAC1 channels (Fig. 2f, grey; Extended Data Fig. 2e). Compared to bulk analysis, immobilized liposomes showed a slightly lower protein occupancy (Fig. 2f) and an enrichment of smaller vesicles (Extended Data Figure 4d). This enrichment of small vesicles, also noted in previous studies [18,25,26], is likely due to their faster diffusion, which promotes more efficient immobilization. We conclude that our single-vesicle setup enables both direct quantification and functional assessment of protein content.

Visualization of phospholipid scrambling by cross-linked VDAC1 in single vesicles

Under our standard reconstitution conditions, crosslinked VDAC1 (henceforth CL-VDAC1) exhibits scramblase activity in cuvette experiments, whereas non-crosslinked

VDAC1 (henceforth NCL-VDAC1) does not [12]. To generate CL-VDAC1, we treated Alexa647-labeled VDAC1 with EGS, an amine-reactive homo-bifunctional crosslinker, generating a sample with a significant proportion of crosslinked protein (Extended Data Fig. S2d). When reconstituted and assayed in bulk via the BSA-back-extraction assay, this preparation displayed expected scramblase activity, while NCL-VDAC1 was inactive (Extended Data Fig. 2f). The CL-Alexa647-VDAC1 preparations used in our experiments consist of a roughly equal mixture of crosslinked and non-crosslinked protein (Extended Data Fig. 2d). To refine our analysis and measure the rate of lipid scrambling catalyzed by a single VDAC1 dimer, we purified the crosslinked dimer fraction (henceforth pCL) by size-exclusion chromatography (Extended Data Fig. 4a) and verified its channel and scramblase activity in cuvette assays (Extended Data Fig. 4b,c).

To visualize scramblase activity in single vesicles, we reconstituted NBD-PC-vesicles with pCL-Alexa647-VDAC1 and introduced these into a TIRF chamber. Vesicles were allowed 1 minute to reach the avidin-coated surface, followed by a 1-minute immobilization pause before imaging (Fig. 1). We used mock-reconstituted liposomes and NCL-Alexa647-VDAC1 proteoliposomes as controls. The buffer flow was started just after the initial image was obtained. Ten images were captured at 90 second intervals, a frequency optimized to minimize photobleaching effects, which accounted for a 1.0 ± 13.4 % (n=63) loss in signal at the end of the image acquisition sequence, as determined using vesicles containing non-extractable head-labeled *N*-NBD-PE (Fig. 2a). After NBD imaging, Alexa647 fluorescence in each vesicle was quantified to estimate VDAC1 content based on initial protein signal as well as Alexa647 photobleaching step analysis.

For protein-free liposomes and NCL-Alexa647-VDAC1 proteoliposomes, decay of NBD fluorescence stabilized in ~100 s, reaching a plateau (determined at 900 s) at 47 ± 10 % (n=254) and 42 ± 9% (n=283), respectively (Fig. 3a and 3b). This indicates the expected loss of only outer-leaflet NBD-PC, consistent with the absence of scrambling in these control samples. In contrast, proteoliposomes reconstituted with pCL-Alexa647-VDAC1 showed deep fluorescence reduction, indicating that inner-leaflet NBD-PC was translocated to the outer leaflet and subsequently lost from the vesicle.

The greatest extents of reduction within the 900 second assay window corresponded to vesicles with high protein content (Fig. 3c). For simplified presentation, we grouped fluorescence traces by VDAC1 content based on Alexa647 fluorescence, with category averages displayed in Fig. 3d-f. These results indicate that our experimental platform enables clear visualization of the protein-dependent scramblase activity of pCL-Alexa647-VDAC1 in single vesicles.

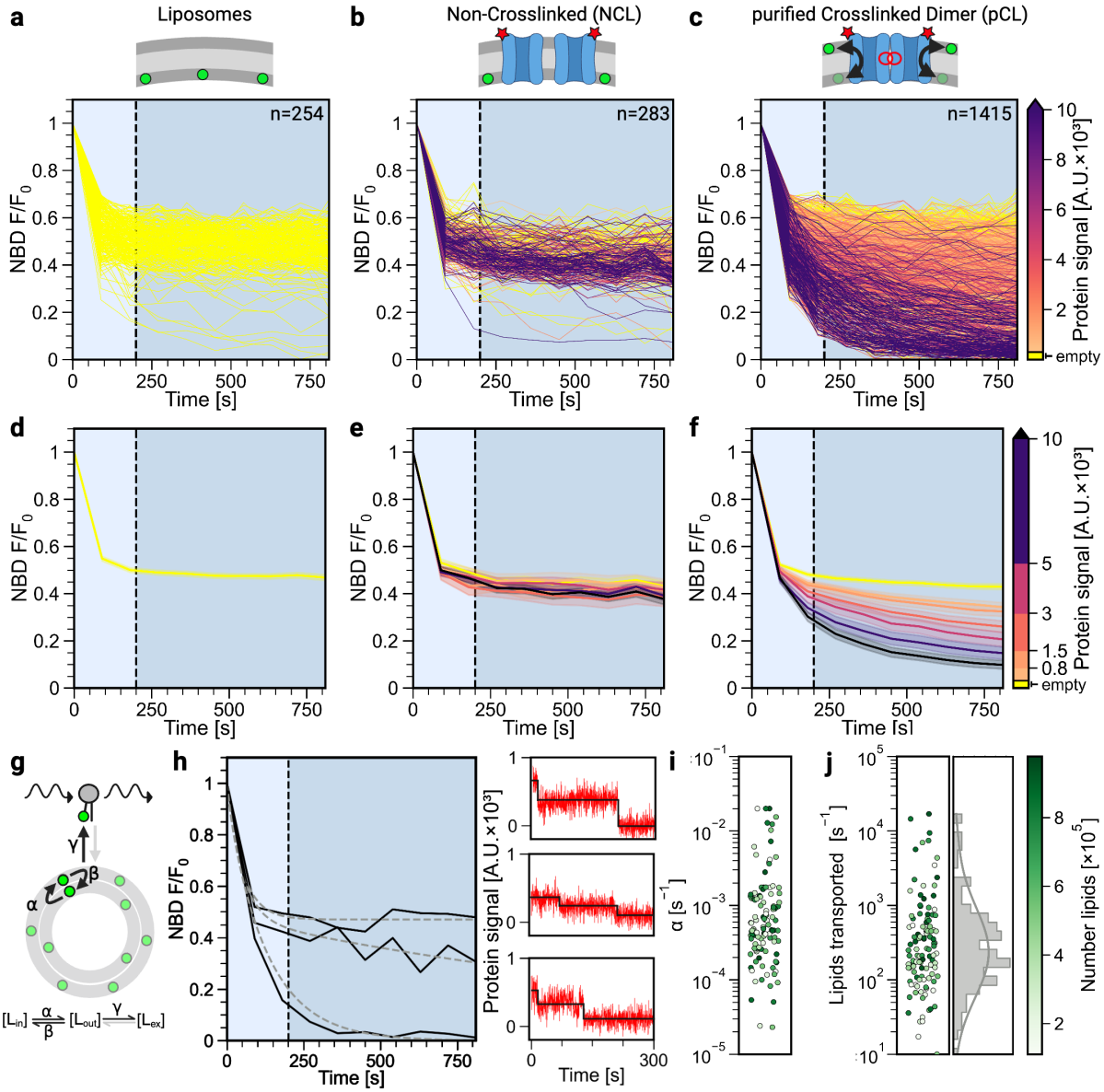

Figure 3. Single vesicle analysis of VDAC1-mediated scramblase activity. 14:0-6:0 NBD-PC proteoliposomes containing either non-crosslinked (NCL) or purified crosslinked (pCL) Alexa647-labeled VDAC1 dimers, as well as protein-free NBD-PC liposomes were immobilized and subjected to TIRF microscopy as illustrated in Fig. 1e. Imaging was started just before buffer flow (t=0 min). Panels show time-resolved comparison of lipid signal for (**a,d**) protein-free liposomes, (**b,e**) NCL-VDAC1 proteoliposomes, and (**c, f**) pCL-VDAC1 dimer proteoliposomes. For each individual liposome, lipid fluorescence intensity is shown as a normalized line plot relative to the initial fluorescence. Protein occupancy in each liposome is

color-coded based on Alexa647 signal intensity, as indicated by the colormap on the right. **d - f**, Fluorescence traces from vesicles with similar protein occupancy were grouped and plotted in increasing order of protein contents, with the protein signal and intensity grouping indicated by the colormap on the right. **g**, Schematic representation of the three-compartment model used for data fitting, illustrating the inner leaflet (L_{in}), outer leaflet (L_{out}) and extracted pool (L_{ex}), along with the respective rate constants. **h**, Representative NBD-fluorescence intensity traces (solid lines) fitted using the three-compartment model (dashed lines) for three single vesicles exhibiting two-step Alexa647 photobleaching events (panels on the right), indicative of the presence of a single pCL-VDAC1 dimer in the vesicles. **i**, Scrambling rate for active vesicles with a single pCL-VDAC1 dimer. Symbols are color-coded to indicate number of lipids per vesicle according to the color map in panel j. **j**, Number of transported lipids per second for individual vesicles with a single pCL-VDAC1 dimer, color-coded to indicate number of lipids per vesicle according to the color map on the right with histogram illustrating the distribution of values. **i - j** The colormap represents the total number of lipids for each vesicle, deduced from initial NBD fluorescence intensity (see Extended Data Fig. 4).

Unitary rate of scrambling by a VDAC1 dimer

To derive the scrambling rate from the traces shown in Figure 3c, we built a three-compartment kinetic model (Fig. 3g, Supplementary information) comprising two pools of fluorescent NBD-PC (L_{in} and L_{out}, representing lipids in the inner and outer leaflet of a single vesicle, respectively) and a third pool (L_{ex}) representing NBD-PC molecules that desorb from the outer leaflet and are removed by buffer flow. Notably, the L_{ex} pool does not contribute to the vesicle fluorescence. To avoid overfitting as each trace has only 10 data points, we assumed that scramblase-mediated exchange between the L_{in} and L_{out} pools occurs at a similar rate in both directions, described by the rate constant α (= β). Furthermore, we constrained γ to 0.01–0.02 s^{-1} (based on the NBD-PC desorption rate in liposomes ($\gamma = 0.012 \pm 0.005\ s^{-1}$; Extended Data Fig. 1g) and set the initial $L_{out}/(L_{in} + L_{out})$ ratio between 45–55%.

Our model yielded high-quality fits ($r^2 > 0.8$), but notably the data revealed significant heterogeneity in scrambling rates with only a weak correlation between protein content and scrambling efficiency (Extended Data Fig. 4f, although protein occupancy increased with vesicle diameter (Extended Data Fig. 4e)). This variability likely arises from differences in dimer interfaces generated during EGS crosslinking. Thus, we previously showed that the scrambling rate is extremely sensitive to the nature of the interface – for example, coarse-grained molecular dynamics simulations indicated robust scrambling by an optimal VDAC1 dimer, while slight rotations of the individual protomers away from this optimal interface, generated interfaces with fivefold reduced scramblase activity. Likewise, we previously identified a VDAC1

variant which formed dimers/multimers in the membrane, but these were unproductive as the construct failed to scramble lipids [12]. Thus, the presence of low-activity vesicles in the single-vesicle dataset likely reflects those reconstituted with VDAC1 dimers with suboptimal interfaces. Moreover, as adding more VDAC1 dimers to a vesicle in the protein/phospholipid ratio regime of our experiments does not necessarily create more active scramblases, this explains the weak correlation between protein signal and scrambling rate.

To determine the scrambling rate of an optimal dimer, we analyzed vesicles where Alexa647 fluorescence exhibited two-step photobleaching, i.e., vesicles containing a single dimer. These vesicles had Alexa647 initial plateau intensities in the range 400–1,000 units, aligning with the average last step height of ~400 ±150 units for photobleaching traces (Extended Data Fig. 5) and consistent with our earlier estimate of a ~ 300 units threshold for a monomer. Three exemplary kinetic traces from this group (Fig. 3h; additional examples in Extended Data Fig. 6) illustrate highly active, slightly active, and inactive dimers. The scrambling rate distribution (Fig. 3i) revealed that the top 20% of vesicles, containing optimal dimers, exhibited rates >0.003 s^{-1}. Combining this information with vesicle size estimates determined using NBD-PC intensity and dynamic light scattering (Extended Data Fig. 4d), and deduced phospholipid content estimates, we obtain a unitary scrambling rate of >1,000 phospholipids per second per VDAC1 dimer for the active subpopulation (Fig. 3j).

Discussion

We developed a quantitative, high-throughput fluorescence imaging platform with surface-immobilized liposomes to determine the precise unitary rate at which phospholipids are scrambled by VDAC1 dimers. This platform allows for the direct observation of individual proteoliposomes, overcoming the limitations of traditional ensemble-averaged methods such as fluorescence-based assays performed on a bulk population of liposomes in a cuvette (Extended Data Fig. 2f and Extended Data Fig. 4c). These conventional approaches suffer from significant sample heterogeneity due to variations in vesicle size, number of proteins reconstituted per vesicle, protein activity and membrane composition, making it difficult to extract accurate kinetic parameters for individual scramblases. In contrast, our approach allows the simultaneous measurement of several hundred individual proteoliposomes, yielding a

robust and statistically rich dataset comprising thousands of single vesicles per sample (Extended Data Fig. 4e). This method is technically simple and highly scalable, using surface immobilization to ensure stable observation over long periods of time. By resolving individual proteoliposomes, we achieve unprecedented accuracy in determining unitary scrambling rates of VDAC1 dimers, revealing kinetic heterogeneity that would be masked in ensemble measurements.

Although native dimers form due to the high abundance of VDAC1 in the outer mitochondrial membrane [15], we purified VDAC1 as a monomer and therefore made use of EGS cross-linking and size-exclusion chromatography to generate and purify a mixture of structurally distinct VDAC1 dimers, each of which is predicted to have a unique protein-protein interface and different scrambling abilities. We reconstituted this mixture into liposomes and used stepwise photobleaching (Fig. 3h and Extended Data Fig. 6) to identify vesicles containing a single dimer. By applying a three-compartment mathematical model to analyze lipid exchange kinetics (Fig. 3g) and correlating this with measurements of vesicle diameter and thereby phospholipid content (Extended Data Fig. 4d), we found that individual dimers exhibited a wide range of scrambling rates, from <100 lipids s^{-1} to >10,000 lipids s^{-1}. The median rate for all active dimers (~200 lipids s^{-1}) aligns with estimates from ensemble measurements (Fig. 3h-j; Jahn 2023). Poorly active and inactive VDAC1 dimers (Fig. 3h), as well as inactive VDAC1 monomers (Fig. 3b, e, and Extended Data Fig. 2f), serve as essential controls, confirming that our reconstitution approach accurately reflects specific protein-mediated scrambling. While bulk assays are often constrained by the need to compare controls that have been treated as similarly as possible to the experimental samples, our approach benefits from an internal control within the sample itself. Specifically, the presence of empty liposomes and inactive dimers within the crosslinked dimer population provides an intrinsic reference.

Our findings support molecular dynamics simulations [12], which predict that rapid scrambling occurs at specific VDAC1 dimer interfaces. The distribution of unitary scrambling rates we observed for VDAC1 dimers is somewhat lower than the ensemble-averaged rates reported for constitutively active GPCR scramblases and Ca^{2+}-activated TMEM16 proteins [27]. This suggests that the VDAC1 dimer interface, formed between two β-barrel protomers, may provide an intrinsically slower pathway for lipid transit, yet still sufficient to support mitochondrial membrane biogenesis [12,28].

With this experimental platform established, future research can focus on (i) characterizing structurally defined VDAC1 dimers generated via site-specific crosslinking to determine their unitary scrambling rates, and (ii) testing different membrane lipid compositions that more closely mimic the mitochondrial outer membrane to evaluate their effect on scrambling activity.

Traditional phospholipid scrambling assays often use the reducing agent dithionite to eliminate NBD-fluorescence in the outer leaflet of unilamellar vesicles [20], allowing scramblase-mediated lipid translocation to be monitored. However, dithionite is unsuitable for measuring VDAC1 dimer scrambling, as it can pass through the VDAC1 pore (Fig. 2d). Nevertheless, within our imaging platform, dithionite-based assays could be adapted to measure non-pore-forming scramblases. In such an approach, vesicles reconstituted with long-chain phospholipids labeled at the headgroup with dithionite-sensitive NBD (Fig. 2a) or ATTO488 [29] could be exposed to dithionite in a flow chamber (Fig. 2d), and the fluorescence decay kinetics analyzed to infer scrambling rates. A similar mathematical framework to that in Figure 3g could be applied, with γ representing the pseudo-first-order rate constant for fluorophore reduction. Given that γ for dithionite reactions is ~0.05 s^{-1} (NBD) and ~0.2 s^{-1} (ATTO488), this method could extend the dynamic range for measuring fast scramblases beyond the ~0.01 s^{-1} limit observed here (Extended Data Fig. 1g).

Beyond its application to VDAC1, our imaging platform can be directly adapted for studying Ca^{2+}-activated scramblases. The outer leaflet NBD-PC probe can be extracted by buffer flow prior to the start of the experiment, so that our workflow starts with the inner leaflet probe only, with flushing of a Ca^{2+} buffer to start the scramblase and allow monitoring of scramblase kinetics. Furthermore, our approach can be readily adapted to measure single-protein transport kinetics of ATP-driven flippases, which transport lipids from the exofacial site to the cytosolic site at inherently slow rates due to their reliance on ATP hydrolysis. As these proteins reconstitute preferably 'inside-out' with their ATPase domains facing outwards [18], their activity could be selectively initiated by introducing ATP into the flow chamber, providing an additional experimental control for functional validation. Here, imaging would begin after extraction of the outer leaflet fluorophores together with a buffer flush supplemented with ATP-Mg or ATP-Na as a control. While bulk measurements require high concentrations of active protein for meaningful readouts, single vesicle microscopy allows selective analysis of the

protein-containing subpopulation, enabling more refined and quantitative assessment even in samples with low protein abundance, bypassing the bottleneck of purification. Substrate specificity, dependence on membrane curvature and ultimately the question of whether flippases operate with on and off states similar to proton pumps [30] could be addressed.

In summary, our high-throughput fluorescence imaging platform provides an unprecedented ability to measure unitary phospholipid scrambling rates of VDAC1 dimers at the single-molecule level. By overcoming the limitations of ensemble-averaged methods, we revealed significant kinetic heterogeneity between individual dimers and validated key predictions from molecular dynamics simulations. Ultimately, our method provides a versatile and scalable tool for dissecting the mechanisms of lipid transport with unparalleled precision.

Methods

Materials

POPC (#850457), POPG (#840457), 14:0-6:0 NBD-PC (#810122), N-NBD-DOPE (#810145), and Biotin-PEG(2000)-DSPE (#880129) were purchased from Avanti polar lipids Inc. (Birmingham, AL, USA). Bio-Gel P-6 media (#1504130) and Bio-Spin chromatography column (#7326008) were purchased from Bio-Rad. Alexa647 C2 Maleimide (#A20347), ethylene glycol bis(succinimidyl succinate) (EGS; #21565), and Micro BCA™ Protein Assay Kit (#53235) were purchased from Thermo Fisher Scientific (Waltham, MA USA). Fatty acid-free bovine serum albumin was purchased from Calbiochem (#126609). For surface coating, PLL(20)-g[3.5]-PEG(2) and PLL(20)-g[3.5]-PEG(2)/PEG(3.4)-biotin(20%) from SUSOS (Dübendorf, Switzerland) were used. All other chemicals and reagents, including Tetramethylrhodamine-5-maleimide (#94506), dithionite (#157953), and the zwitterionic detergent N,N-Dimethyl-n-dodecylamine N-oxide (LDAO; #40236) were obtained from Sigma, if not stated otherwise.

VDAC1 purification and fluorescence labeling

PCR-based site-directed mutagenesis was used to engineer a single amino acid change (A170C) in a cysteine-less VDAC1 (C127S, C232S) background, generating

the VDAC1-A170C construct (referred to here simply as VDAC1). This construct was expressed in chemically competent BL21 (DE3)-omp9 *E. coli* and purified from inclusion bodies as described previously, using Ni-NTA affinity chromatography followed by size exclusion [12,31] For labeling, 170-340 µg of purified VDAC1 (100 µL of a 50-100 µM VDAC1 solution in 20 mM Tris-HCl, pH 8.0, 150 mM NaCl, 0.1 % (w/v) LDAO) was reacted with a 10-fold molar excess of Alexa647 C_2 Maleimide (from a 10 mM stock solution in DMSO) or mock-treated with DMSO. Samples were incubated for 2 h at 40°C and 650 rpm in an Eppendorf Thermomixer, then treated with dithiothreitol to react with free dye, followed by a 15 min-incubation (dithiothreitol was added from a 1 M stock solution to give a 20-fold molar excess over Alexa647 C_2 Maleimide). Samples were desalted three times using 1 mL of Bio-Gel P-6 in Bio-Spin columns equilibrated in crosslinking buffer (10 mM MOPS-KOH pH 7.0, 100 mM KCl, 0.05% LDAO). Protein concentration was quantified using absorbance at 280 nm (ε_{280} = 32,500 M^{-1} cm^{-1}) as well as the Micro BCA™ Protein Assay Kit, with a typical recovery of 23 ± 2% (mean ± SD, n=4) after desalting. To quantify labeling efficiency, small aliquots of equivalent amounts of Alexa647-treated and unlabeled VDAC1 were treated with tetramethylrhodamine-5-maleimide (added in 10-fold excess from a 0.2 mM stock in DMSO) following the same protocol. As tetramethylrhodamine is smaller than Alexa647 it is expected to react quantitatively with solvent-accessible cysteines. Rhodamine-labeled samples were analyzed by SDS-PAGE followed by visualization and labelling quantification using the Bio-Rad ChemiDoc™ MP Imaging System. This protocol indicated that that Alexa647 labeling was 97 ± 3% efficient (mean ± SD, n = 2) as ~3% of the sample could be additionally labeled with rhodamine.

Preparation of liposomes

Large unilamellar vesicles (LUVs) composed of POPC, POPG (9:1, molar ratio), 0.5 mol% 14:0-6:0 NBD-PC and 0.1 mol% Biotin-PEG(2000)-DSPE were prepared in reconstitution buffer (10 mM MOPS/KOH pH 7.0, 100 mM KCl) following Jahn et al., 2023, yielding a preparation with a typical phospholipid concentration of 3.5 mM. For control experiments 0.5 mol% *N*-NBD-DOPE was used instead of 14:0-6:0 NBD-PC. The LUVs had a hydrodynamic diameter of 183 ± 13 nm and polydispersity of 11% ± 4% (mean ± SD, n=5), as determined by Dynamic Light Scattering using an Anton Paar Litesizer™ 500 Particle Analyzer. To prepare vesicles with 14:0-6:0 NBD-PC located exclusively in the outer leaflet (asymmetrically labeled vesicles), NBD-PC was

left out of the original liposome preparation and added afterwards. Briefly, 12 µg 14:0-6:0 NBD-PC were dissolved in 1 µL ethanol and 9 µL reconstitution buffer, and 2 µL of this solution were added to 50 µL unlabeled liposomes, diluted with reconstitution buffer to a total volume of 100 µL. The sample was incubated on ice for 10 min to ensure complete outside labeling and subsequently used for measurements. For TIRF microscopy, symmetrically labeled liposomes were diluted 1:15,000 and asymmetrically labeled liposomes were diluted 1:7,500 in reconstitution buffer.

Crosslinking, reconstitution into LUVs, and bulk assays

Alexa Fluor™ 647-labeled VDAC1 was crosslinked with EGS or mock-treated with DMSO and reconstituted into preformed NBD-PC-containing LUVs as described [12,31]. For reconstitution, 800 µL vesicles and 2-15 µg Alexa Fluor™ 647-labeled VDAC1 were used. Phospholipid concentration of the reconstituted vesicles was typically 2.5 mM and dynamic light scattering indicated a hydrodynamic diameter of 247 ± 38 nm and polydispersity of 15 ± 5% (intensity-weighted size distribution, mean ± SD, n=24). Proteoliposomes and protein-free mock-treated liposome controls were assayed for channel activity using dithionite, and scramblase activity using fatty acid-free bovine serum albumin by fluorescence-based bulk assays In some experiments, EGS-crosslinked multimers were resolved from monomers by size exclusion chromatography using a Superdex 200 Increase 10/300 GL column run in 20 mM Tris-HCl, pH 8.0, 150 mM NaCl, 0.1 % (w/v) LDAO. Fractions were analyzed by SDS-PAGE, and in-gel Alexa647 fluorescence was used to identify the most enriched multimer fraction, which was then reconstituted into liposomes as described above, yielding vesicles with a hydrodynamic diameter of 203 ± 9 nm and polydispersity of 15 ± 5% (intensity-weighted size distribution, mean ± SD, n=3).

Glass slide cleaning and coating

Glass coverslips (26 x 76 mm, thickness #1.5, Thermofisher) were sonicated twice for 15 min in 2 % (v/v) Hellmanex III solution, thoroughly rinsed with ddH_2O, then sonicated in methanol and stored in fresh methanol. After drying with compressed air, coverslips were ozone-cleaned for 15 min using a Novascan PSD Pro UV Ozone system (Novascan technologies, Boone, IA, USA). A bottomless 6-channel sticky slide (Sticky-Slide VI 0.4, ibidi GmbH, Gräfelfing, Germany) was adhered to the cleaned

coverslip (channels: 17 x 3.8 x 0.4 mm, 30 µL channel capacity, 60 µL per well). The channels were flushed with 60 µL of 1 mg/mL Biotinyl-PLL-PEG/PLL- PEG (1:1,000) in PBS (150 mM NaCl, 8 mM Na_2HPO_4, 2 mM KH_2PO_4, pH 7.0). After 20 min, unbound material was removed by flushing the channels 5 times with 60 µL of reconstitution buffer. Biotin groups were saturated by flushing with 60 µL of 0.025 g/L NeutrAvidin in reconstitution buffer, incubated for 20 min, then flushed 5 times with 60 µL of reconstitution buffer to remove unbound fraction. The dish was used immediately for microscopy or stored at 4ºC for up to a week.

TIRF microscopy

Image acquisition was performed using an inverted TIRF microscope (IX83, Olympus, Hamburg, Germany) with a 100x oil-immersion objective (1.5 NA; Olympus), an Orca-flash 4.0 sCMOS camera (Hamamatsu Photonics K.K., Hamamatsu, Japan), and a quad band emission filter cube (DAPI/FITC/CY3/CY5). Lasers were aligned and refocused before each session. NBD fluorophores were excited using a 488 nm laser at 10% intensity (18.3 mW/cm^2) with 25 ms exposure time and the Alexa647 protein marker was excited with a 640 nm laser at 15% intensity (20.2 mW/cm^2) and 200 ms exposure time. Both laser angles were adjusted to 200 nm penetration depth. To avoid uncertainty at the edges of the illuminated area, the central 1,024 x 1,024-pixel region, corresponding to 66.56 × 66.56 µm in 16-bit range, was used for analysis, resulting in a pixel size of 65 × 65 nm. The IX-ZDC z-drift compensator (Olympus) maintained the focal plane during long-term imaging.

Single vesicle phospholipid scramblase assay

Measurements were made at ambient temperature. Tubing (Masterflex Tygon E-lab L/S 13; Bohlender PTFE 0.5 x 1.0 mm, I.D x O.D) was connected to the wells of the channel slide for buffer flow using a peristaltic LabV1 pump with an AMC2 head (Drifton, Hvidovre, Denmark). The tubing and channel were flushed with reconstitution buffer for 1 min (20 rpm, 500 µL/min), followed by flushing the buffer-diluted sample (1:1,500) for 1 min at 500 µl/min After 1-minute incubation for immobilization, time-lapse imaging started with buffer flush (500 µl/min, RT) starting immediately after the first image. Using the CellSens experiment manager (Version 3.2; Olympus), one image was taken every 90 s in the lipid channel, with up to a total of 10 images in 15

min. Subsequently, the same frame was repeatedly imaged 1,250 times in the red channel for photobleaching step analysis.

Single vesicle dithionite assay to determine vesicle occupancy

The experimental setup was similar to the single vesicle scramblase assay. After sample immobilization, a 5-min buffer flush removed all accessible outer leaflet short-chain NBD lipids. Using a multi-position imaging tool, 12 frames were analyzed simultaneously as described previously [18].Three imaging rounds, each capturing three images per frame in both channels, were performed. After the first round, reconstitution buffer containing 10 mM dithionite (from a 1 M stock in 0.5 M Tris pH 10) was flushed through the channel for 1 min followed by 2 min incubation. After the second round, alamethicin (10 µM, prepared in 10 mM dithionite) was flushed for 1 min with additional 2 min incubation to ensure completion of alamethicin-induced permeabilization and dithionite quenching before the final imaging round.

Data analysis

Recorded .vsi/.ets files were converted to TIFF format in FIJI (2.9.0/1.52v) using bio-formats reader with batch processing without interpolation. TIFF files were analyzed with a custom Python algorithm based on [18]. Particle centers and corresponding intensity maxima were tracked in the lipid channel TIFF stack using *trackpy* [32], with local background-corrected intensities extracted using *photutils* and *astropy* [33]. Particle coordinates determined from the lipid channel were used to extract protein channel signals from the same regions. Lipid and protein thresholds were optimized using a protein free sample. As described in detail in the Results section, lipid fluorescence of scramblase-containing proteoliposomes decays rapidly at first, corresponding to the loss of outer leaflet lipids to the flow of buffer, and then more slowly as lipids from the inner leaflet are scrambled out and lost to buffer flow in turn. Vesicles with no lipid signal decrease upon buffer flow were excluded from analysis, as well as vesicles decreasing too rapidly indicative of detaching. The extraction rate constant, i.e., the rate of loss of outer leaflet lipids to buffer flow, was determined by fitting traces from protein-free liposomes to a mono-exponential function (see Extended Data Fig. 1f,g). The extraction rate γ was constrained to the bounds 0.01-0.02 s^{-1} and the initial outer to inner leaflet NBD-lipid distribution to the bounds 0.045-

0.55, respectively when fitting fluorescence decay traces for scramblase active-proteoliposomes based on a three compartment model adapted from [24] using *scipy* (see Supplementary information). To estimate vesicle size based on lipid signal, the lipid signal intensity distribution average was normalized by the sample average determined by DLS (Extended Data Fig. 4d) as described previously [18,34]. Figures were created with BioRender software (https://biorender.com).

Data availability

Source data are provided with this paper.

Code availability

Home written analysis code is described in detail in the Methods. Code is available upon reasonable request.

Acknowledgements

We thank Indu Menon for Extended Data Figure 1E and Joshua Levitz for feedback and comments. Imaging data were collected at the BioChemical Imaging Facility (Ruhr University Bochum). This work was supported by the National Institutes of Health (grant no. R01GM146011 to A.K.M.) and the Deutsche Forschungsgemeinschaft (grant no. VE 1674/1-1 to S.V.; grant nos. GU 1133/13-1 and INST 213/985-1 to T.G.P.).

Author contributions

S.V., A.K.M. and T.G.P. conceived the study. K.M.M. contributed the three-compartment model. G.I.D. and F.N. prepared samples and performed bulk assays, S.V. performed, analyzed, and wrote software for single-vesicle experiments, under the supervision of A.K.M. and T.G.P.; and S.V., A.K.M. and T.G.P. wrote the manuscript and discussed it with all authors.

Competing interests

The authors declare no competing interests.

Additional information

Extended data is provided with the manuscript.

Supplementary information is provided with the manuscript.

References

1. Jan, L. Y. & Jan, Y. N. Wide-ranging cellular functions of ion channels and lipid scramblases in the structurally related TMC, TMEM16 and TMEM63 families. *Nat Struct Mol Biol* **32**, 222–236 (2025).
2. Pomorski, T. & Menon, A. K. Lipid flippases and their biological functions. *Cell Mol Life Sci* **63**, 2908–21 (2006).
3. Pomorski, T. G. & Menon, A. K. Lipid somersaults: Uncovering the mechanisms of protein-mediated lipid flipping. *Prog Lipid Res* **64**, 69–84 (2016).
4. Sakuragi, T. & Nagata, S. Regulation of phospholipid distribution in the lipid bilayer by flippases and scramblases. *Nat Rev Mol Cell Biol* 1–21 (2023) doi:10.1038/s41580-023-00604-z.
5. Sanyal, S. & Menon, A. K. Flipping lipids: why an' what's the reason for? *ACS Chem Biol* **4**, 895–909 (2009).
6. Sebinelli, H. G., Syska, C., Čopič, A. & Lenoir, G. Established and emerging players in phospholipid scrambling: A structural perspective. *Biochimie* **227**, 111–122 (2024).
7. Wang, Y. & Kinoshita, T. The role of lipid scramblases in regulating lipid distributions at cellular membranes. *Biochem Soc Trans* **51**, 1857–1869 (2023).
8. Menon, I. *et al*. Opsin is a phospholipid flippase. *Curr Biol* **21**, 149–153 (2011).

9. Suzuki, J., Umeda, M., Sims, P. J. & Nagata, S. Calcium-dependent phospholipid scrambling by TMEM16F. *Nature* **468**, 834–838 (2010).
10. Malvezzi, M. *et al.* Ca2+-dependent phospholipid scrambling by a reconstituted TMEM16 ion channel. *Nat Commun* **4**, 2367 (2013).
11. Reinisch, K. M. & Prinz, W. A. Mechanisms of nonvesicular lipid transport. *J Cell Biol* **220**, e202012058 (2021).
12. Jahn, H. *et al.* Phospholipids are imported into mitochondria by VDAC, a dimeric beta barrel scramblase. *Nat Commun* **14**, 8115 (2023).
13. Acoba, M. G., Senoo, N. & Claypool, S. M. Phospholipid ebb and flow makes mitochondria go. *J Cell Biol* **219**, e202003131 (2020).
14. Joshi, A., Richard, T. H. & Gohil, V. M. Mitochondrial phospholipid metabolism in health and disease. *J Cell Sci* **136**, jcs260857 (2023).
15. Gonçalves, R. P., Buzhysnskyy, N. & Scheuring, S. Mini review on the structure and supramolecular assembly of VDAC. *J Bioenerg Biomembr* **40**, 133–138 (2008).
16. Larsen, J., Hatzakis, N. S. & Stamou, D. Observation of Inhomogeneity in the Lipid Composition of Individual Nanoscale Liposomes. *J. Am. Chem. Soc.* **133**, 10685–10687 (2011).
17. Menon, I. *et al.* A cholesterol switch controls phospholipid scrambling by G protein-coupled receptors. *Journal of Biological Chemistry* 105649 (2024) doi:10.1016/j.jbc.2024.105649.
18. Veit, S. *et al.* Single Vesicle Fluorescence-Bleaching Assay for Multi-Parameter Analysis of Proteoliposomes by Total Internal Reflection Fluorescence Microscopy. *ACS Appl. Mater. Interfaces* **14**, 29659–29667 (2022).

19. Watanabe, R., Sakuragi, T., Noji, H. & Nagata, S. Single-molecule analysis of phospholipid scrambling by TMEM16F. *Proceedings of the National Academy of Sciences* **115**, 3066–3071 (2018).
20. Chang, Q., Gummadi, S. N. & Menon, A. K. Chemical Modification Identifies Two Populations of Glycerophospholipid Flippase in Rat Liver ER. *Biochemistry* **43**, 10710–10718 (2004).
21. Kubelt, J., Menon, A. K., Müller, P. & Herrmann, A. Transbilayer Movement of Fluorescent Phospholipid Analogues in the Cytoplasmic Membrane of *Escherichia coli*. *Biochemistry* **41**, 5605–5612 (2002).
22. Lyons, J. A., Timcenko, M., Dieudonné, T., Lenoir, G. & Nissen, P. P4-ATPases: how an old dog learnt new tricks — structure and mechanism of lipid flippases. *Current Opinion in Structural Biology* **63**, 65–73 (2020).
23. Herrera, S. A. & Günther Pomorski, T. Reconstitution of ATP-dependent lipid transporters: gaining insight into molecular characteristics, regulation, and mechanisms. *Biosci Rep* **43**, BSR20221268 (2023).
24. Marx, U. *et al.* Rapid Flip-Flop of Phospholipids in Endoplasmic Reticulum Membranes Studied by a Stopped-Flow Approach. *Biophysical Journal* **78**, 2628–2640 (2000).
25. Hatzakis, N. S. *et al.* How curved membranes recruit amphipathic helices and protein anchoring motifs. *Nat Chem Biol* **5**, 835–841 (2009).
26. Olsson, T., Zhdanov, V. P. & Höök, F. Total internal reflection fluorescence microscopy for determination of size of individual immobilized vesicles: Theory and experiment. *Journal of Applied Physics* **118**, 064702 (2015).

27. Malvezzi, M. *et al*. Out-of-the-groove transport of lipids by TMEM16 and GPCR scramblases. *Proc. Natl. Acad. Sci. U.S.A.* **115**, (2018).

28. Petrungaro, C. & Kornmann, B. Lipid exchange at ER-mitochondria contact sites: a puzzle falling into place with quite a few pieces missing. *Current Opinion in Cell Biology* **57**, 71–76 (2019).

29. Mathiassen, P. P. M., Menon, A. K. & Pomorski, T. G. Endoplasmic reticulum phospholipid scramblase activity revealed after protein reconstitution into giant unilamellar vesicles containing a photostable lipid reporter. *Sci Rep* **11**, 14364 (2021).

30. Veshaguri, S. *et al.* Direct observation of proton pumping by a eukaryotic P-type ATPase. *Science* **351**, 1469–73 (2016).

31. Dearden, G. I., Ravishankar, V., Sakata, K., Menon, A. K. & Bergdoll, L. Protocol for the production and reconstitution of VDAC1 for functional assays. *STAR Protocols* **5**, 103240 (2024).

32. Allan, D. B., Caswell, T., Keim, N. C., van der Wel, C. M. & Verweij, R. W. soft-matter/trackpy: Trackpy v0.5.0. Zenodo https://doi.org/10.5281/zenodo.4682814 (2021).

33. Bradley, L. *et al.* astropy/photutils: 1.2.0. (2021) doi:10.5281/zenodo.5525286.

34. Lohr, C., Kunding, A. H., Bhatia, V. K. & Stamou, D. Constructing Size Distributions of Liposomes from Single-Object Fluorescence Measurements. in 143–160 (Elsevier, 2009). doi:10.1016/S0076-6879(09)65008-4.

Extended Data

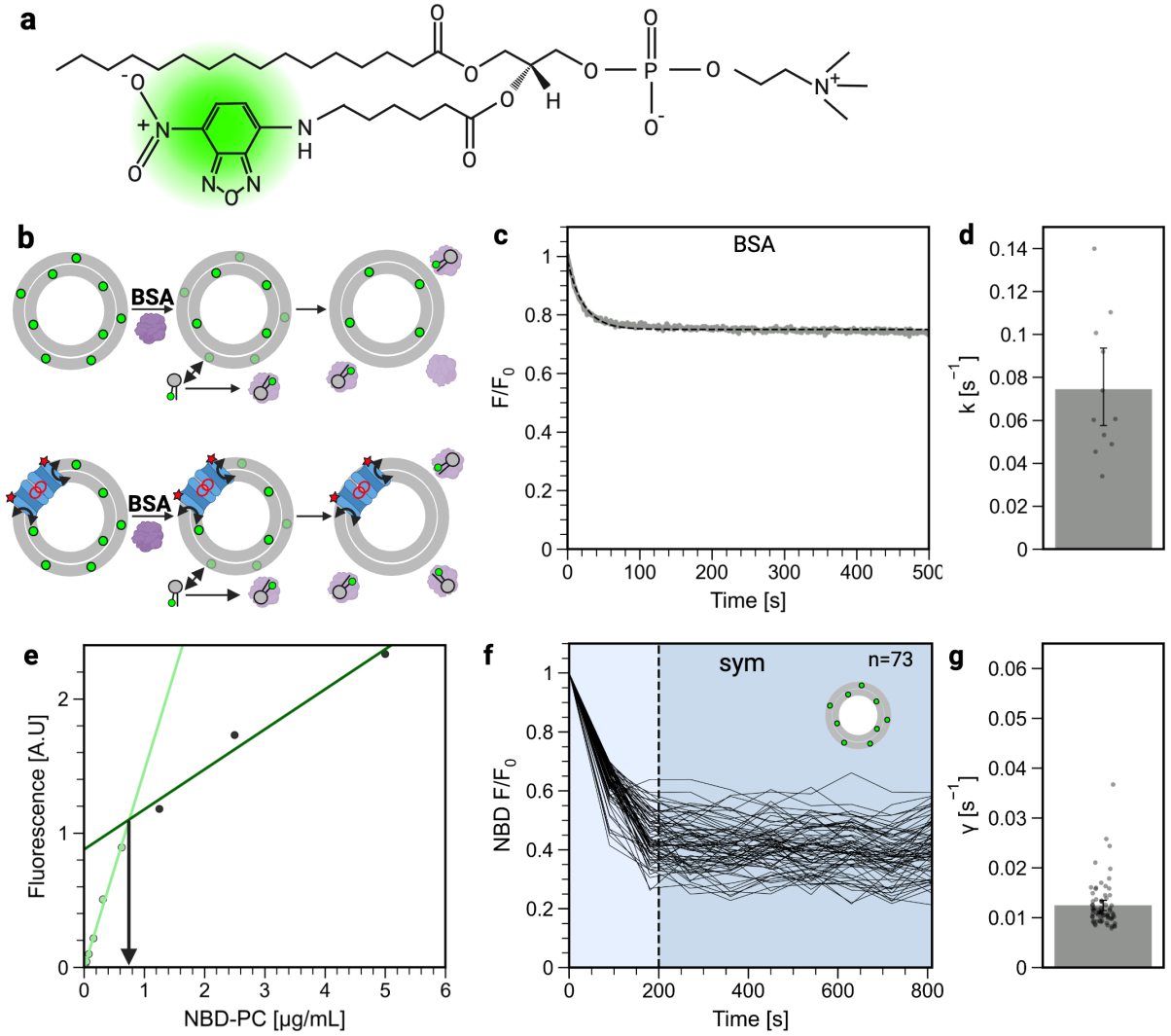

Extended Data Figure 1. Determination of lipid extraction rate. a, Structure of 14:0-6:0 NBD-PC. **b**, Scheme of BSA cuvette assay. Fatty acid-free BSA is added to a suspension of vesicles in a cuvette. Short-chain NBD-labeled lipids in the outer leaflet of the vesicles partition into the aqueous phase, where they bind to BSA. As the fluorescence quantum yield of the NBD fluorophore is ~2-fold lower when NBD-PC is bound to BSA versus located in the membrane, a drop in fluorescence is observed. In vesicles with a functioning scramblase, inner-leaflet lipids translocate outward and are captured by BSA, resulting in a greater drop in fluorescence compared with protein-free liposomes. This assay enables real-time measurement of lipid translocation and extraction kinetics. **c**, Time-course analysis of cuvette BSA assay on symmetrically 14:0-6:0 NBD-PC labeled, protein-free liposomes, expressed as normalized fluorescence intensity relative to the initial value, following the addition of excess BSA. The desorption process is monitored by measuring the decrease in fluorescence over time, which reflects the transfer of NBD-PC from the liposomal membrane to BSA in solution. **d**, Kinetic analysis of NBD-PC desorption from protein-free liposomes. Fluorescence decay traces were fitted to a monoexponential decay function (for example, dashed line in panel c), yielding a rate constant of k = 0.07 s^{-1}, corresponding to the desorption kinetics of the 14:0-6:0 NBD-PC probe (n = 11). **e**, Fluorescence intensity as a function of NBD-PC concentration in an aqueous environment, used to determine its solubility threshold (0.75 µM) as the point at which monomeric NBD-PC self-associates, resulting in a change in fluorescence quantum

efficiency. This point was determined as the intersection of two lines corresponding to linear fits of the two portions of the graph. **f**, Symmetrically labeled liposomes were immobilized and just after initial TIRF microscopy image was taken (t=0 min), buffer flow was started. For each vesicle, lipid fluorescence signals were normalized to their respective initial intensities, Representative traces show the time-dependent loss of 14:0-6:0 NBD-PC fluorescence from individual symmetrically labeled vesicles. **g**, The fluorescence decay traces from (f) were fitted to a monoexponential decay function. The desorption rate constant (γ) was determined for each individual vesicle (dots), yielding an average desorption rate of 0.0124 ± 0.0045 s^{-1} (mean ± S.D.).

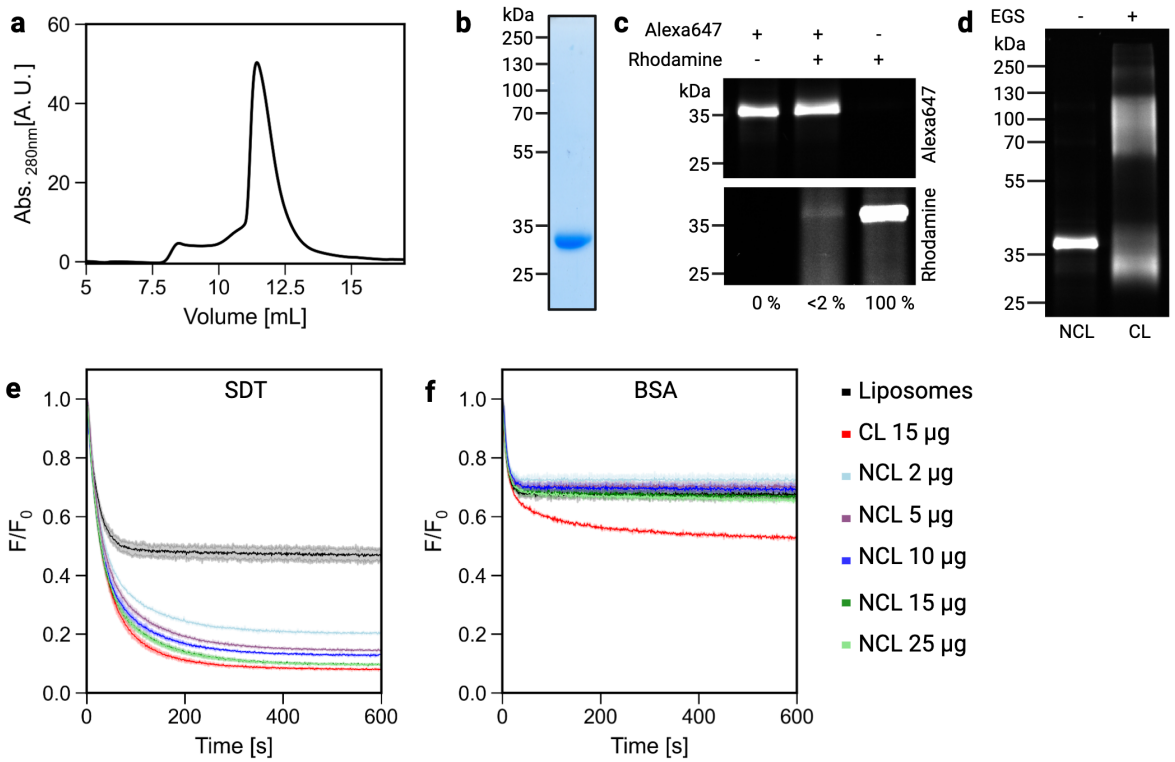

Extended Data Figure 2. VDAC1-A170C purification, labeling and crosslinking. a, Size exclusion chromatography profile of purified VDAC1-A170C. **b**, Coomassie-stained SDS-PAGE of peak fraction. **c**, Purified VDAC1-A170C was labeled via Alexa647-maleimide, and subsequently labeled with rhodamine-maleimide to detect any unreacted cysteines. Only 1.3 % of the preparation remained susceptible to modification by the second label, indicating high efficiency (>97 ± 3%; mean ± SD, n = 2) of the initial Alexa647 conjugation. An SDS-PAGE gel is shown, imaged to visualize Alexa647 (top panel) or rhodamine (lower panel). **d**, Purified, Alexa647-labeled VDAC1 was either mock-treated with DMSO or crosslinked using EGS to generate stable dimers/multimers. An SDS-PAGE gel is shown, imaged to visualize Alexa647. **e - f**, Suspensions of protein-free 14:0-6:0 NBD-PC liposomes or proteoliposomes reconstituted with the indicated amounts of either non-crosslinked (NCL) or crosslinked (CL) Alexa647-labeled VDAC1 were subjected to dithionite (SDT) reduction or BSA back extraction assays in a cuvette (the SDT assay reports the fraction of vesicles reconstituted with a VDAC1 channel, whereas the BSA assay reports the fraction of vesicles with scramblase activity); **e**, Time-course analysis of 14:0-6:0 NBD-PC fluorescence (normalized to the starting value) in liposomes and VDAC1-containing vesicles upon dithionite addition; **f**, Time-course analysis of 14:0-6:0 NBD-PC fluorescence (normalized to the starting value) in liposomes and VDAC1-vesicles upon BSA addition.

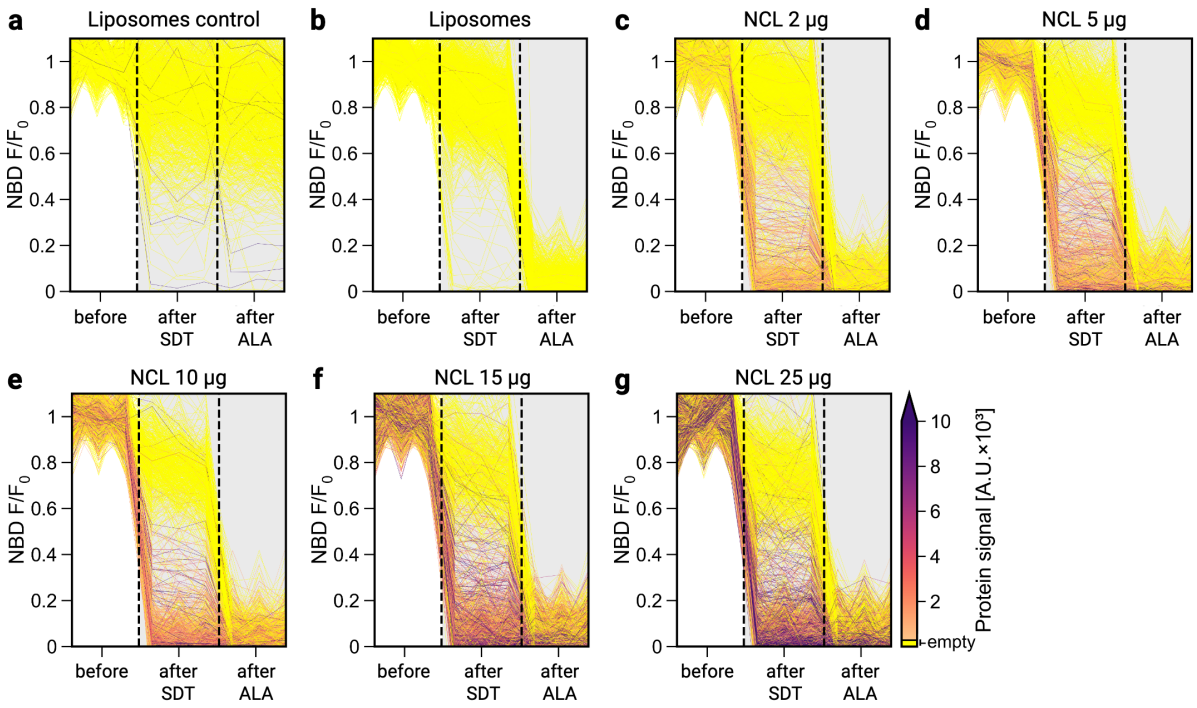

Extended Data Figure 3. Single vesicle dithionite assay to determine VDAC1 occupancy. Protein-free 14:0-6:0 NBD-PC liposomes or 14:0-6:0 NBD-PC proteoliposomes reconstituted with indicated amounts of non-crosslinked (NCL) Alexa647-VDAC1 were immobilized and subjected to a single-vesicle dithionite assay. To remove NBD-PC from the outer leaflet, vesicles were flushed for 5 min before imaging. Three 'before' images were taken, followed by flushing with 10 mM sodium dithionite (SDT) for 1 min followed by 2 min incubation at the first dashed line in each plot, after which 'after SDT' images were taken. Subsequently, alamethicin in 10 mM SDT was flushed for 1 min with 2 min incubation (second dashed line), and 'after ALA' images were acquired to assess further NBD-PC fluorescence bleaching due to vesicle permeabilization. Each trace represents the change in NBD-PC fluorescence intensity from single vesicles, with protein signals color-coded according to the colormap shown to the right of panel g. Protein-free liposomes were measured either without additions to estimate photobleaching (a) or with additions (b). Fluorescence traces for single proteoliposomes containing non-crosslinked VDAC1 are shown in (c-g).

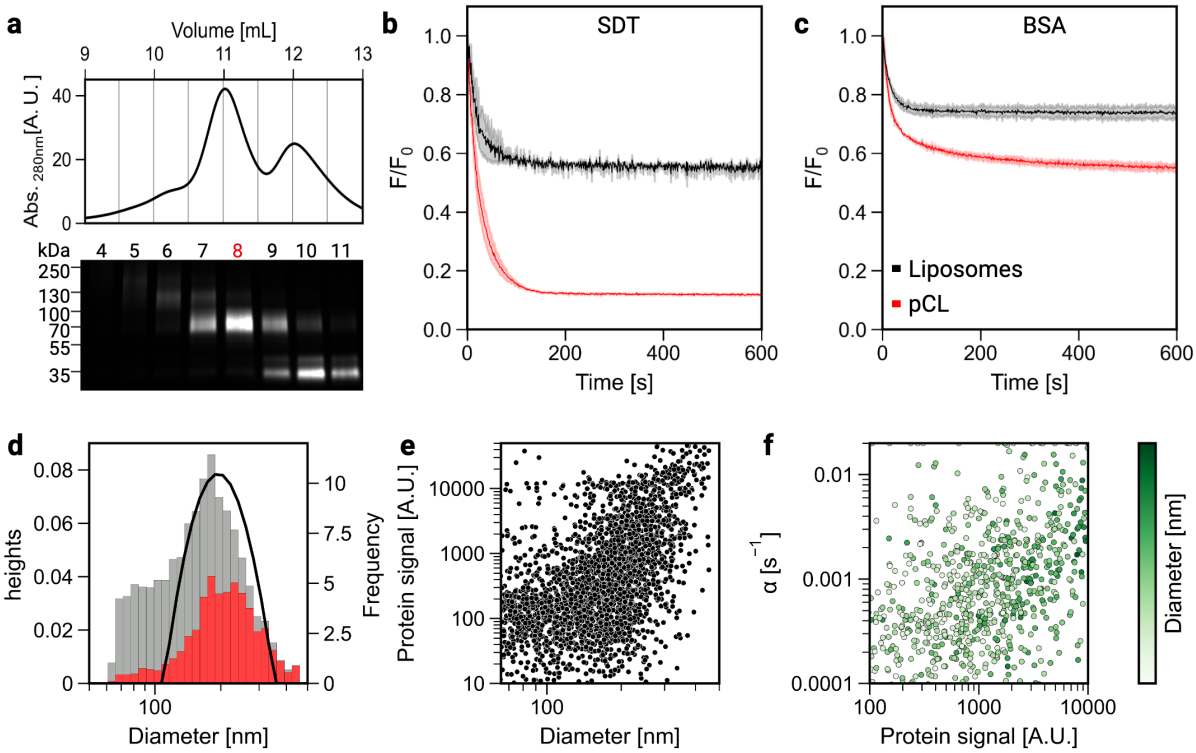

Extended Data Figure 4. Characterization of purified VDAC1 dimer proteoliposomes (pCL). a, Size-exclusion chromatography elution profile of EGS-crosslinked Alexa647-labeled VDAC1 (top panel) and an Alexa647 fluorescence image of an SDS-PAGE gel of collected fractions (bottom panel). Fraction 8, highly enriched in VDAC1 dimers (pCL, purified dimer) was used for reconstitution into NBD-PC liposomes to yield pCL proteoliposomes. **b,** Bulk cuvette-based sodium dithionite (SDT) and **c**, BSA assays comparing proteoliposomes with pCL VDAC1 dimers with mock-reconstituted liposomes. **d**, Dynamic light scattering intensity distribution, revealing an average vesicle diameter of 203 nm (solid line). The lipid fluorescence intensity distribution histogram of the sample obtained via TIRF microscopy, normalized by DLS measurements, with vesicles categorized as protein-containing (red) or empty (grey). **e**, Correlation analysis of protein signal intensity versus lipid signal intensity, assessing the dependence of protein occupancy on vesicle diameter. **f**, Values of the scrambling rate constant (alpha, see Fig. 3g), derived from single-vesicle traces fitted to the three-compartment kinetic model, plotted against initial protein fluorescence signal of the vesicles. Data points are color-coded by vesicle diameter, based on lipid signal normalized via DLS.

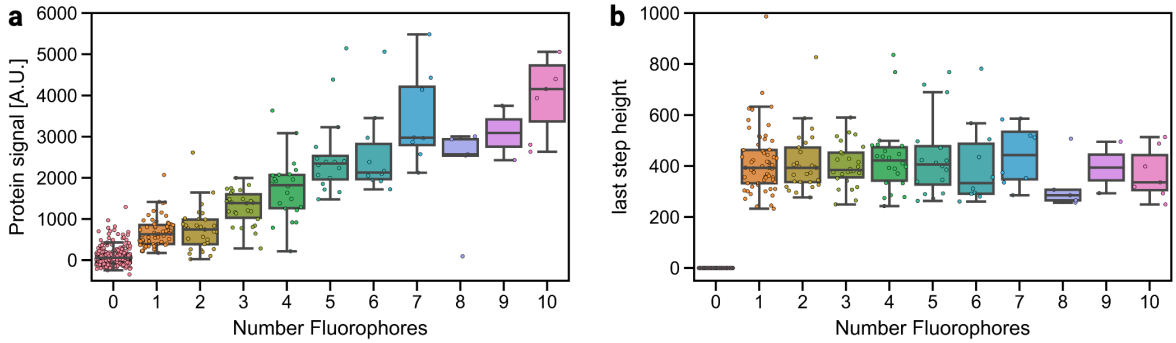

Extended Data Figure 5. Single Alexa647 fluorophore intensity determined by bleaching steps. 14:0-6:0 NBD-PC proteoliposomes containing pCL Alexa647-labeled VDAC1 were immobilized and subjected to photobleaching step analysis using TIRF microscopy. **a**, Initial protein fluorescence signal of each vesicle is plotted against the total number of detected fluorophores per vesicle, determined by discrete photobleaching steps. This analysis provides insight into the fluorophore occupancy within individual proteoliposomes. Note that the fitting success is reduced with increasing fluorophore number. **b**, Final photobleaching step intensity, categorized by fluorophore count per vesicle, represents single-fluorophore emission, ranging from ~250–550 A.U.

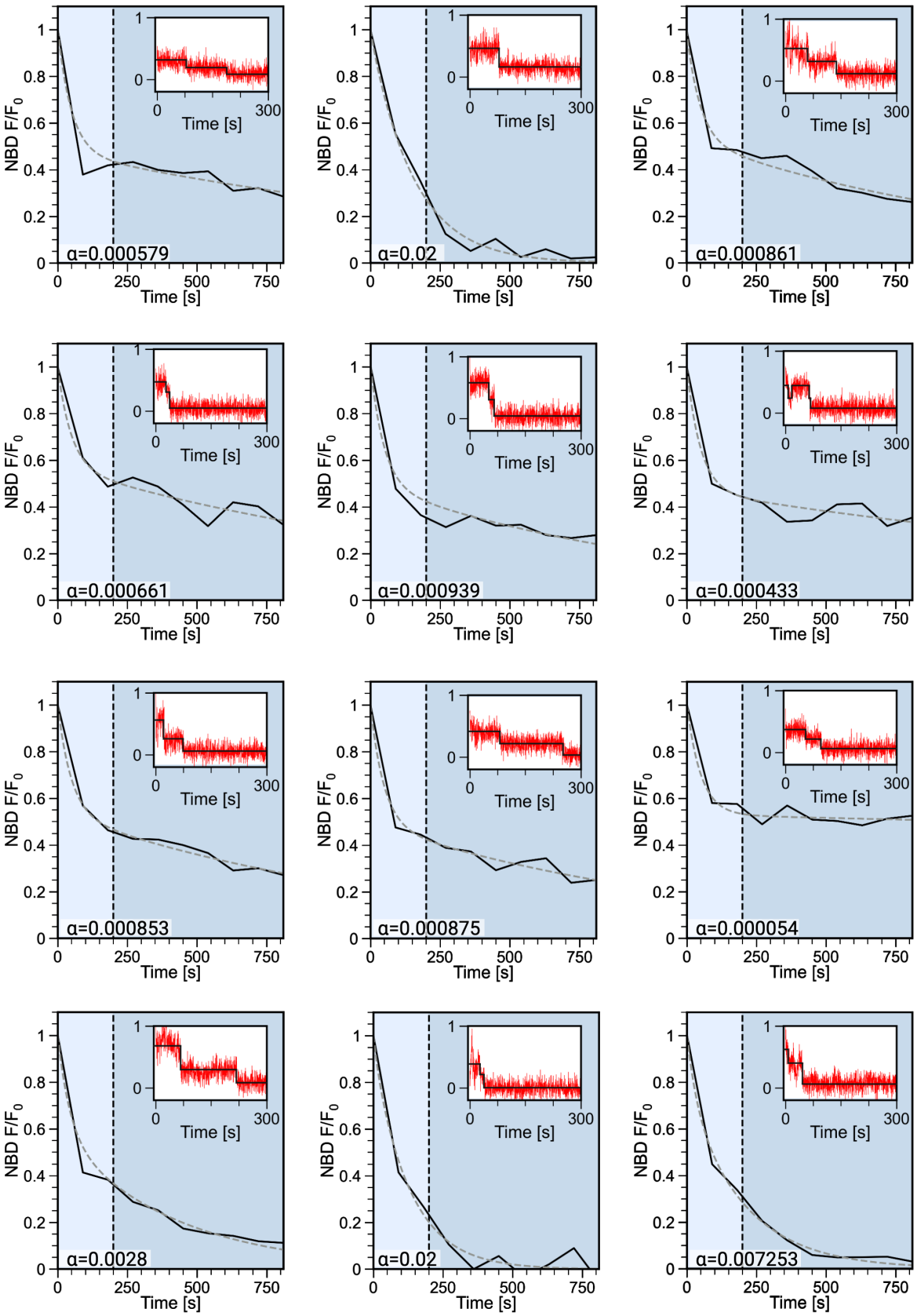

Extended Data Figure 6. Exemplary traces for proteoliposomes containing one pCL VDAC1 dimer. 14:0-6:0 NBD-PC proteoliposomes containing pCL Alexa647-labeled VDAC1 were immobilized and subjected to TIRF microscopy. Imaging was started just before buffer

flow (t=0 min). For each individual liposome, lipid fluorescence intensity is shown as a normalized line plot relative to the initial fluorescence. The scramblase kinetic parameter α was determined using a three-compartment model (fit shown as dashed line) and is displayed in the lower-left corner. The *Inset* shows the corresponding photobleaching step analysis for the protein fluorophores.

Kinetics Calculations

Sarina Veit[1], Grace I. Dearden[2], Kartikeya M. Menon[3], Faria Noor[2], Anant K. Menon[2], Thomas Günther Pomorski[1,4]

[1]Department of Molecular Biochemistry, Faculty of Chemistry and Biochemistry, Ruhr University Bochum, Bochum 44801, Germany
[2]Department of Biochemistry, Weill Cornell Medical College, New York, New York, 10021, USA
[3]Icahn School of Medicine at Mount Sinai, New York, NY 10029
[4]Department of Plant and Environmental Sciences, University of Copenhagen, DK-1871 Frederiksberg C, Denmark

Nomenclature

$L_{in}(t)$	Inner leaflet NBD lipid pool
$L_{out}(t)$	Outer leaflet NBD lipid pool
$L_{ex}(t)$	Extracted NBD lipid pool
α, β	Forward and backward scrambling rate constants
γ	Rate constant of NBD fluorophore extraction
$\mathbf{R}$	Coefficient matrix of $L_{in}(t)$ and $L_{out}(t)$ system
λ_i	Eigenvalues of $\mathbf{R}$
$\mathbf{v}_i$	Eigenvectors of $\mathbf{R}$
$\mathbf{I}_2$	Identity matrix dimension 2

1. Problem Definition

A three-compartment (L_{in}, L_{out}, L_{ex}) model is used to determine the rate constants for scrambling (α, β) and for buffer extraction (γ). The kinetic model for bilayer lipid distribution (inner leaflet: L_{in}, outer leaflet: L_{out}) and reduction (L_{ex}) is as follows:

$$\mathrm{L_{in}(t)} \underset{\beta}{\overset{\alpha}{\rightleftharpoons}} \mathrm{L_{out}(t)} \xrightarrow{\gamma} \mathrm{L_{ex}} \tag{1}$$

The evolution in time t of the three-compartment model is defined with a system of differential equations:

$$\frac{\mathrm{d}L_{in}(t)}{\mathrm{d}t} = L'_{in}(t) = -\alpha L_{in}(t) + \beta L_{out}(t) \tag{2}$$

$$\frac{\mathrm{d}L_{out}(t)}{\mathrm{d}t} = L'_{out}(t) = \alpha L_{in}(t) + (-\beta - \gamma) L_{out}(t) \tag{3}$$

$$\frac{\mathrm{d}L_{ex}(t)}{\mathrm{d}t} = L'_{ex}(t) = \gamma L_{out}(t) \tag{4}$$

The following initial conditions are assumed:

$$L_{ex}(t=0) = 0; L_{in}(t=0) + L_{out}(t=0) = 1 \tag{5}$$

To solve this 3-compartment model, only equations (2) and (3) need to be considered, as the formation of $L_{ex}(t)$ is independent of $L_{in}(t)$ and does not affect the dynamics of the 2×2 system. (If preferred, in the equivalent formulation in terms of a Markov chain, $L_{ex}(t)$ represents an absorbing state and doesn't need to be solved directly).

This system can be represented in matrix form:

$$\begin{pmatrix} L'_{in}(t) \\ L'_{out}(t) \end{pmatrix} = \begin{pmatrix} -\alpha & \beta \\ \alpha & -(\beta+\gamma) \end{pmatrix} \begin{pmatrix} L_{in}(t) \\ L_{out}(t) \end{pmatrix} \tag{6}$$

This is a 2×2 homogeneous system of first order ordinary differential equations, alternatively shown as: $\mathbf{L}'(t) = \mathbf{R}\mathbf{L}(t)$. The general solution takes the form:

$$\mathbf{L}(t) = \begin{pmatrix} c_1 v_{11} e^{\lambda_1 t} + c_2 v_{12} e^{\lambda_2 t} \\ d_1 v_{21} e^{\lambda_1 t} + d_2 v_{22} e^{\lambda_2 t} \end{pmatrix} = \begin{pmatrix} A_1 e^{\lambda_1 t} + A_2 e^{\lambda_2 t} \\ B_1 e^{\lambda_1 t} + B_2 e^{\lambda_2 t} \end{pmatrix} \tag{7}$$

2. Computing Eigenvalues and Eigenvectors

Eigenvalues of the homogeneous system are the roots of the characteristic equation, solved below:

$$\det(\mathbf{R} - \lambda \mathbf{I}_2) = \begin{vmatrix} -\alpha - \lambda & \beta \\ \alpha & -(\beta + \gamma + \lambda) \end{vmatrix} = 0 \tag{8}$$

$$(-\alpha - \lambda)(-\beta - \gamma - \lambda) - \alpha\beta = 0 \tag{9}$$

$$\lambda^2 + (\alpha + \beta + \gamma)\lambda + \alpha\gamma = 0 \tag{10}$$

$$\lambda = \frac{-(\alpha + \beta + \gamma) \pm \sqrt{(\alpha + \beta + \gamma)^2 - 4\alpha\gamma}}{2} \tag{11}$$

Eigenvectors $\mathbf{v}_i$ arise from the 2×2 system

$$(\mathbf{R} - \lambda_i \mathbf{I}_2)\mathbf{v}_i = \mathbf{0}$$

Where v_{11} and v_{21} are components of eigenvector $\mathbf{v}_1$, the example equation below can be solved for both eigenvectors.

$$(-\alpha - \lambda_1)v_{11} + \beta v_{21} = 0$$
$$\alpha v_{11} + (-\beta - \gamma - \lambda_1)v_{21} = 0$$

$$(\mathbf{v}_1\mathbf{v}_2) = \begin{pmatrix} \beta & \beta \\ \alpha + \lambda_1 & \alpha + \lambda_2 \end{pmatrix} \tag{12}$$

These eigenvectors can be equivalently computed by substituting equation (7) into the original system of differential equations (6):

$$\begin{pmatrix} L'_{in}(t) \\ L'_{out}(t) \end{pmatrix} = \begin{pmatrix} \lambda_1 A_1 e^{\lambda_1 t} + \lambda_2 A_2 e^{\lambda_2 t} \\ \lambda_1 B_1 e^{\lambda_1 t} + \lambda_2 B_2 e^{\lambda_2 t} \end{pmatrix} = \begin{pmatrix} -\alpha & \beta \\ \alpha & -(\beta + \gamma) \end{pmatrix} \begin{pmatrix} A_1 e^{\lambda_1 t} + A_2 e^{\lambda_2 t} \\ B_1 e^{\lambda_1 t} + B_2 e^{\lambda_2 t} \end{pmatrix} \tag{13}$$

Simplifying this equation leads to equivalent eigenvector construction as in the solution above:

$$A_1(\lambda_1 + \alpha)e^{\lambda_1 t} + A_2(\lambda_2 + \alpha)e^{\lambda_2 t} = \beta B_1 e^{\lambda_1 t} + \beta B_2 e^{\lambda_2 t} \tag{14}$$

$$B_1 = A_1 \frac{\lambda_1 + \alpha}{\beta} \tag{15}$$

$$B_2 = A_2 \frac{\lambda_2 + \alpha}{\beta} \tag{16}$$

For more compact notation, f_i is defined:

$$f_i = \frac{\alpha + \lambda_i}{\beta} \tag{17}$$

3. Solving Initial Conditions

The remaining unknowns in the expression of bilayer lipid concentrations are A_1 and A_2. These variables are calculated using the initial condition assumptions laid out in Section 1.

$$L_{in}(t) = A_1 e^{\lambda_1 t} + A_2 e^{\lambda_2 t} \tag{18}$$

$$L_{out}(t) = B_1 e^{\lambda_1 t} + B_2 e^{\lambda_2 t} = \frac{\alpha + \lambda_1}{\beta} A_1 e^{\lambda_1 t} + \frac{\alpha + \lambda_2}{\beta} A_2 e^{\lambda_2 t} \tag{19}$$

$$L_{in}(t = 0) + L_{out}(t = 0) = 1 \tag{20}$$

A_1 and A_2 can be solved by substitution:

$$L_{in}(t=0) = A_1 + A_2 \tag{21}$$

$$L_{out}(t=0) = B_1 + B_2 = f_1 A_1 + f_2 A_2 \tag{22}$$

$$L_{out}(t=0) = f_1(L_{in}(t=0) - A_2) + f_2 A_2 \tag{23}$$

$$L_{out}(t=0) - f_1 L_{in}(t=0) = A_2(f_2 - f_1) \tag{24}$$

$$\tag{25}$$

$$A_2 = \frac{f_1 L_{in}(t=0) - L_{out}(t=0)}{f_1 - f_2} \tag{26}$$

$$A_1 = \frac{L_{out}(t=0) - f_2 L_{in}(t=0)}{f_1 - f_2} \tag{27}$$

As the reaction between L_{out} and L_{ex} is irreversible, computing an additional term for A_1 and A_2 for such an inhomogeneous system is not necessary.

4. Modeling

The final formulae used for regression incorporate all these derived terms and the initial condition assumption in (5) that fluorophores are split between the inner and outer leaflets at time $t = 0$.

$$L_{in}(t) = \frac{1 - f_2}{2(f_1 - f_2)} e^{\lambda_1 t} + \frac{f_1 - 1}{2(f_1 - f_2)} e^{\lambda_2 t} \tag{28}$$

$$L_{out}(t) = \frac{f_1 - f_1 f_2}{2(f_1 - f_2)} e^{\lambda_1 t} + \frac{f_1 f_2 - f_2}{2(f_1 - f_2)} e^{\lambda_2 t} \tag{29}$$

Using Python 3.11.6 and SciPy 1.15.0, the total fluorescence $F(t) = L_{in}(t) + L_{out}(t)$ can be fitted against time t with nonlinear least squares to identify α, β, and γ. As each experiment has 10 data points, $n/10$ parameters can be reasonably fit for bias-variance trade-off, so a univariate fit for α was performed. The initial split of fluorophores between the inner and outer leaflets was allowed to vary between 0.45 and 0.55 in the univariate model for α.